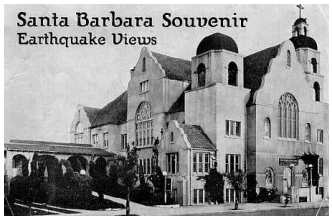


*4th IASPEI / IAEE International Symposium:*

**Effects of Surface Geology on Seismic Motion**

August 23–26, 2011 · University of California Santa Barbara

# DYNAMIC DEFORMATIONS FROM SEISMICITY NEAR THE ITOIZ RESERVOIR, NORTHERN SPAIN

**Miguel A Santoyo[1], Patricia Martínez-Garzón[1]*, Antonio García-Jerez[2], Francisco Luzón[2] and Miguel Herraiz[1].**

1 Depto. Física de la Tierra, Astronomía y Astrofísica I. Facultad de Ciencias Físicas, Universidad Complutense de Madrid. Spain.
2 Grupo de Geofísica Aplicada. Departamento de Física Aplicada. Universidad de Almería, Spain.
* Now at: Deutsches GeoForschungsZentrum (GFZ). Telegrafenberg, 14473 Potsdam, Germany

ABSTRACT

We calculate and analyze the time histories of the 3D displacement gradients and dynamic deformations due to seismicity near the Itoiz reservoir, in Navarra, northern Spain. The seismic data here used, were obtained by means of a temporal network recently installed by the University of Almería, with broadband and accelerometric stations. Seismic sensors were located on the surface and at underground sites in the vicinity of the dam. The dynamic deformation field is calculated using two different methods. First, a seismo-geodetic approach using data from a three-station micro-array located close to the dam structure. Second, by single station estimates of the displacement gradients, assuming the incidence of body wave fields propagating through the seismic recording site. The dynamic deformations obtained from both methods are compared and analyzed in the context of the local effects near the dam. The shallow 1D velocity structure near the dam was also estimated from the same seismic data by modeling the seismic recordings from local seismicity. This analysis should help to extend the single station method to other sites of interest with only one station.

Results show that, for the studied earthquakes, the displacement gradients obtained by both methods are quite similar. They also show that the greatest amplitudes of these dynamic deformations are found mainly on the horizontal directions and that rigid body rotations are larger around the vertical rotation axis.

## INTRODUCTION

Some damaging effects produced by earthquakes may be a direct result of strong dynamic deformations (strains and rotations) rather than from peak accelerations or other displacement variations alone (e.g. Clough and Penzien, 1993; Bodin, *et al.,* 1997). An example of this can be found on the extensive damages suffered by Mexico City's water system following the September 19, 1985 Mexico earthquake (Mw=8.1), where one-third of the residents of the metropolitan area were left without water. This damage has been attributed to axial strains in the buried pipelines (Ayala and O'Rourke, 1989). Other types of engineering buried structures such as subways and tunnels usually result damaged after strong earthquake shaking due to high dynamic deformations (e.g. Ariman and Hamada, 1981; Clough and Penzien, 1993). Surface dynamic deformations have been studied in the past for different regions and earthquakes, e.g. Spudich, *et al*., (1995) for the 1992 Landers earthquake; Bodin, *et al.,* (1997) and Singh, *et al.,*(1997) in Mexico City; Gomberg (1997) for the 1994 Northrigde earthquake; Gomberg and Felzer (2008). However few studies of this type have been published for sites near dams in relatively irregular topographies.

Earthquake ground motion near dams is the result of various types of seismicity (regional and local earthquakes), which can produce diverse levels of dynamic stresses and deformations around the dam area. Although few dams have suffered permanent damage after been subjected to intense ground motions (e.g. Koyna dam in India, Hsinfengkiang dam in the People's Republic of China), there is a growing concern about the seismic safety of these critical facilities (e.g. Panel on Earthquake Engineering for Concrete Dams, 1991; Talwani, 1997). In this sense, there is a considerable interest on the evaluation of dynamic deformations near the dam structures. Understanding the dynamic deformations from seismicity may have important implications for seismic engineering and seismic risk assessment.

In this work we calculate the dynamic deformation field in the Itoiz dam, Northern Spain, by means of two different methods. First a seismo-geodetic approach, which uses seismic data from a micro-array of seismic stations, and second by single station estimates of the displacement gradients, assuming the incidence of body waves (S wave field) propagating through the seismic recording site. The seismic data used was obtained by means of a temporal network recently installed by the University of Almería, with broadband and accelerometric stations. Seismic sensors were located on the surface and at underground sites in the vicinity of the dam.

Seismic setting

The Itoiz reservoir is a newly constructed dam located in Navarra, northern Spain in the south-western part of the Pyrenees (Fig. 1). The main geologic units of the region are also shown in Fig. 1. Here, NPZ=North Pynrenean Zone; PAZ=Paleozoic Axial Zone; SPZ=South Pyrenean Zone; NPF=North Pyrenean Fault; PF=Pamplona Fault; CV and A = Paleozoic Basque Massifs; AB=Aquitaine Basin; EB=Ebro Basin; JPB=Jaca-Pamplona Basin. IR = Itoiz Reservoir. This dam stores the water from the Irati and Urrobi rivers. It has a total height of 121.0 m and a total length of 525 m. In this part of the Pyrenees the seismicity during the second half of the last century appears relatively sparse with small to moderate magnitudes and shallow depths (e.g. Ruiz, *et al.*, 2006). From instrumental catalogues, earthquakes show low to moderate magnitudes (up to M=5.5) since the last few decades (Ruiz, *et al*., 2006). However, six destructive earthquakes with intensities greater than VII have been reported in this area in the recent past (Martínez-Solares and Mezcua, 2003). Even when few clustered seismic series in the region have been reported during this period, eight months after the beginning of impoundment of this dam, a clustered seismic series began on September 2004. The series was headed by an Mw=4.7 mainshock, followed by 350 moderate and small aftershocks. The mainshock and the largest aftershock were widely felt in this region and in the western Pyrenees. Ruiz, *et al.,* (2006) report an intensity V in the region of Aoiz and at the Itoiz Dam and an intensity IV in Pamplona City.

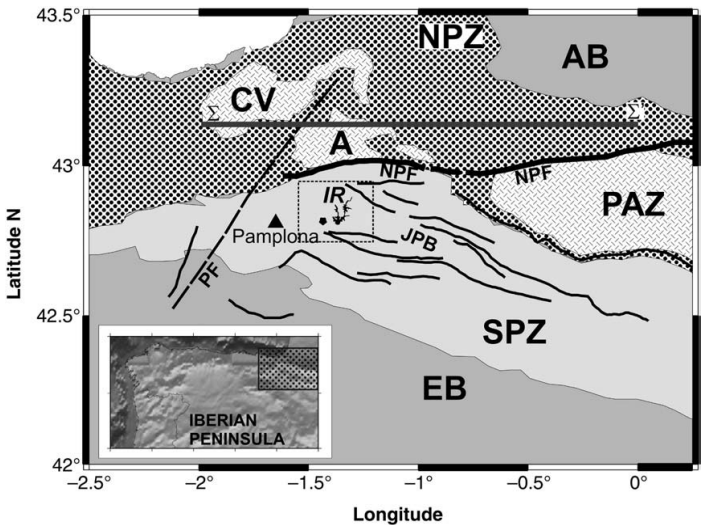


*Fig. 1. Location and geologic setting of the studied zone. NPZ=North Pynrenean Zone; PAZ=Paleozoic Axial Zone; SPZ=South Pyrenean Zone; NPF=North Pyrenean Fault; PF=Pamplona Fault; Paleozoic Basque Massifs: CV=Cinco Villas Massif; A=Aldudes-Quinto Real Massif. AB=Aquitaine Basin; EB=Ebro Basin; JPB=Jaca-Pamplona Basin; IR=Itoiz Reservoir*

METHOD AND DATA

As we mentioned, we apply two methodologies for the analysis of dynamic deformations. The first one based on a seismo-geodetic analysis, which requires the data from a seismic array with at least three three-component seismic stations. A second one based on a single station analysis which, in this case, assumes incidence of S body waves to the recording site.

Seismo-geodetic method

The "seismo-geodetic" analysis to calculate the deformation field at the surface is characterized by the displacement gradient tensor,

obtained from a microarray with at least three thee-component stations. This method is based on the procedure described by Spudich, *et al*. (1995) and Bodin, *et al.* (1997). Here, the displacement gradient tensor $G^g_{i,j}=\partial u_i/\partial x_j$, where i,j=1,2,3 ($x_1$=x=east, $x_2$=y=north, $x_3$=z=up respectively), *g* for seismo-geodetic method, is calculated at each time from the ground displacements $u_i$. $G^g_{i,j}$ is obtained by solving the set of equations

$$\overline{d}^i = G^g_{i,j}\,\overline{R}^i \tag{1}$$

where $\overline{d}^i = \overline{u}^i - \overline{u}^0 = \left(u^i - u^0, v^i - v^0, w^i - w^0\right)$is the relative recorded displacement between the reference station (superscript "*o*") and station "*i*" , and $\overline{R}^i = \overline{r}^i - \overline{r}^0 = \left(x^i - x^0, y^i - y^0, z^i - z^0\right)$is the difference in spatial coordinates between these stations. Once obtained the components of $G^g_{i,j}$, these are used to derive the uniform strains

$$\varepsilon_{i,j} = \frac{1}{2}\left(\frac{\partial u_i}{\partial x_j} + \frac{\partial u_j}{\partial x_i}\right) \tag{2}$$

and the rigid body rotations

$$\omega_{i,j} = \frac{1}{2}\left(\frac{\partial u_i}{\partial x_j} - \frac{\partial u_j}{\partial x_i}\right) \tag{3}$$

where i=1,2,3; j=1,2,3; $u_1$=u, $u_2$=v, $u_3$=w; u, v and w are the displacements in the x, y and z directions at a given time. At the surface, due to the stress free boundary conditions, three components of $G^g_{i,j}$ are not independent: $\partial u_1/\partial x_3 = -\partial u_3/\partial x_1$ , $\partial u_2/\partial x_3 = -\partial u_3/\partial x_2$ and $\partial u_3/\partial x_3 = \eta\,(\partial u_2/\partial x_2 + \partial u_1/\partial x_1)$ and $\eta=-\lambda/(\lambda+2\mu)$; $\lambda$ and $\mu$ are the Lamé Parameters. From here, $\varepsilon_{1,3}=\varepsilon_{3,1}=\varepsilon_{2,3}=\varepsilon_{3,2}=0$. A more detailed procedure to solve this system of equations can be found in e.g. Spudich, *et al.* (1995).

Single-station method

In this method, dynamic deformations are obtained at a single site by using a set of three component velocity seismograms with the assumption of body wave incidence through the recording site.

Assuming the incidence of S body waves, the horizontal particle motion can be written as (e.g. Gomberg 1997; Singh, *et al.*, 1997)

$$u_{SH} = A_{SH}e^{i(\omega t - k_h\cdot r + \theta_{SH})}\ ;\ u_{SVh} = A_{SVh}e^{i(\omega t - k_h\cdot r + \theta_{SVh})} \text{ and } u_{SVv} = A_{SVv}e^{i(\omega t - k_h\cdot r + \theta_{SVv})} \tag{4}$$

where $u_{SH}$ is the SH motion in the transverse direction, $u_{SVh}$ and $u_{SVv}$ are the SV motions in the radial and vertical direction respectively; $A_{SH}$ , $A_{SVh}$ and $A_{SVv}$ are the amplitudes in the transverse, radial and vertical directions and $\theta_{SH}$ , $\theta_{SVh}$ , $\theta_{SVv}$ are the phases of the incident wavefield at the surface in the measurement point. $\omega=2\pi f$ is the angular frequency and *t*= time. Here $\boldsymbol{k_h}\bullet\,\boldsymbol{r} = k_x x + k_y y$ , where the magnitude of the horizontal wavenumber is $k_h=2\pi/\lambda_h$ and $\lambda_h$ is the horizontal wavelength. This one can be expressed as $\lambda_h=TV_s/\sin(\psi)=TV_h$, where *T*=period, $V_s$ is the S wave velocity, $V_h$ is the horizontal apparent velocity and $\psi$ is the angle of wave incidence with respect to the vertical.

The horizontal surface motion can be resolved in the three Cartesian directions as (e.g. Gomberg, 2011)

$$u^x_j = A^x_j e^{i\theta_x} e^{i(\omega t - k_x x)} \text{ and } u^y_j = A^y_j e^{i\theta_y} e^{i(\omega t - k_y y)}\ ;\ j=x,y,z \tag{5}$$

The spatial derivatives of equations *5* are then taken in order to obtain the displacement gradients. The differentiation of the term $e^{-ik_x x}$ is equivalent to multiply by $-ik_x = -i2\pi/\lambda_x = -i(2\pi/\lambda_h)\sin(\phi)$ and the term $e^{-ik_y y}$ equivalent to multiply by $-ik_y = -i2\pi/\lambda_y = -i(2\pi/\lambda_h)\cos(\phi)$, where $\phi$=is the angle of azimuth of the incidence wavefield. The derivative with respect to time is equivalent to multiplication in the frequency domain by $i2\pi/T$. From this, the spatial gradients $G^s_{i,j}$ (*s* for single station) of equations 5, at the measuring site can be written as:

$$U_x = \frac{\partial u_1}{\partial x_1} = -\frac{\partial u_1}{\partial t}\frac{\sin\phi}{V_h} = -\frac{\partial u_1}{\partial t}\frac{\sin\phi\sin\psi}{V_s};\ V_x = \frac{\partial u_2}{\partial x_1} = -\frac{\partial u_2}{\partial t}\frac{\sin\phi}{V_h} = -\frac{\partial u_2}{\partial t}\frac{\sin\phi\sin\psi}{V_s}$$

$$W_x = \frac{\partial u_3}{\partial x_1} = -\frac{\partial u_3}{\partial t}\frac{\sin\phi}{V_h} = -\frac{\partial u_3}{\partial t}\frac{\sin\phi\sin\psi}{V_s};\ U_y = \frac{\partial u_1}{\partial x_2} = -\frac{\partial u_1}{\partial t}\frac{\cos\phi}{V_h} = -\frac{\partial u_1}{\partial t}\frac{\cos\phi\sin\psi}{V_s} \quad (6)$$

$$V_y = \frac{\partial u_2}{\partial x_2} = -\frac{\partial u_2}{\partial t}\frac{\cos\phi}{V_h} = -\frac{\partial u_2}{\partial t}\frac{\cos\phi\sin\psi}{V_s};\ W_y = \frac{\partial u_3}{\partial x_2} = -\frac{\partial u_3}{\partial t}\frac{\cos\phi}{V_h} = -\frac{\partial u_3}{\partial t}\frac{\cos\phi\sin\psi}{V_s}$$

At the surface, due to the stress free boundary conditions, the vertical gradients of $G^s_{i,j}$ can be derived from the horizontal components as: $U_z$=-$W_x$ ; $V_z$=-$W_y$ ; $W_z$=-[$\nu$/(1-$\nu$)] ($U_x$+$V_y$), where $\nu$= Poisson coefficient of the medium at the surface. Again, once obtained the components of $G^s_{i,j}$, these are used to derive the uniform strains and the rigid body rotations by means of equations 2 and 3 (e.g. Martínez-Garzón, 2011).

Data and time series processing

During the year 2008, the University of Almería installed a temporal seismic network in the vicinity of the Itoiz dam, consisting of five accelerometers and five broad-band seismic stations, which were operating for a period of nearly 2 years. Three of these stations: two broad-band (PIAL and PGAL) and one accelerometer (PDAL) were installed in the dam site (Fig. 2). PDAL and PIAL were installed at surface and PGAL in an underground gallery in the left margin of the dam. During the operating period, several local and regional earthquakes were recorded by the network. From the observed local earthquakes, we selected those which were recorded in all the three stations located at the dam site, with its epicenters closer than 10.0 km from the recording sites. This maximum distance was selected in order to have, as possible, a nearly vertical incidence of the wavefield to the station. In this way, it could be ensured that most of the incoming seismic energy would be contained in the S wave-field. In total, we used 8 earthquakes for the study with magnitudes ranging from Ms=0.8 to Ms=1.8. These events occurred between November 2008 and January 2009. The initial epicentral locations of these events were taken from published catalogs of the National Geographical Institute of Spain (IGN) and the Commissariat à l'Energie Atomique (CEA) of France. The parameters of these earthquakes are shown in Table 1.

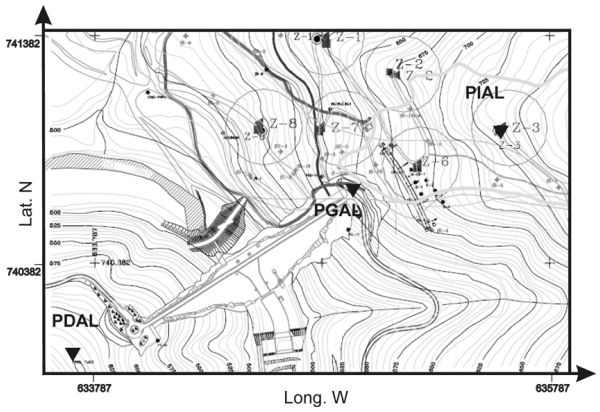


*Fig. 2. Location of recording stations relative to the dam wall. PIAL and PDAL stations are located at surface. PGAL station location is shown by its vertical projection at the surface.*

The recorded time series were first baseline corrected and then band-pass filtered with a 4-pole Butterworth filter in the frequency band of 0.5 Hz<fc<4.0 Hz. The 4.0 Hz upper bound of the filter was selected in order to avoid the possible spatial aliasing from signals with wavelengths significantly smaller than our array. Specifically, to obtain array gradient estimates accurate to approximately 90% of true gradients, the array dimensions must be less than approximately one quarter-wavelength of the dominant energy in the wave train (Bodin, *et al.,* 1997). Given this, the upper bound of the filter should satisfy the relation L≤$\lambda$/4=$V_s$/4f, where L= maximum vertical distance among stations. Satisfying this assures that the deformation field is uniform within the array at any time. Before filtering, data was tapered 5% at the edges of the time histories. After filtering, accelerograms were time-integrated two times and seismograms were time-integrated once in order to obtain the displacement time histories.

Table 1. Parameters of the earthquakes used in this study.

| Event Number | Date | Zs* (km) | M Ms | Epicentral Location | | | | | | | | | |
|---|---|---|---|---|---|---|---|---|---|---|---|---|---|
| | | | | IGN | | | | | CEA | | | | |
| | | | | Lat (º) | Lon (º) | Smaj (km) | Smin (km) | Az (º) | Lat(º) | Lon(º) | Smaj (km) | Smin (km) | Az(º) |
| 885470 | 18/11/08 | 2 | 1,6 | 42,8081 | -1,3645 | 2,1 | 0,9 | 30 | 42,8 | -1,35 | 2,0 | 1,5 | 2,7 |
| 885487 | 19/11/08 | 2 | 1,6 | 42,8084 | -1,3628 | 1,2 | 0,7 | 8 | 42,81 | -1,37 | 1,2 | 1,0 | 6,9 |
| 885493 | 19/11/08 | 2 | 1,2 | 42,8089 | -1,3610 | 1,2 | 0,8 | 10 | 42,8 | -1,36 | 1,8 | 1,1 | 179,1 |
| 885494 | 19/11/08 | 2 | 0,8 | 42,8097 | -1,3565 | 1,4 | 1,1 | 150 | 42,79 | -1,34 | 1,4 | 0,8 | 2,3 |
| 890543 | 23/12/08 | 2 | 1,4 | 42,8055 | -1,3606 | 1,4 | 0,8 | 168 | 42,8 | -0,135 | 1,9 | 1,2 | 160,3 |
| 890840 | 25/12/08 | 2 | 1,6 | 42,8069 | -1,3610 | 1,2 | 0,8 | 171 | 42,82 | -1,37 | 2,5 | 2,0 | 169,2 |
| 891920 | 1/9/09 | | 1,3 | 42,8146 | -1,3606 | 2,7 | 2,1 | 141 | | | | | |
| 893160 | 1/19/09 | | 1,4 | 42,8070 | -1,3557 | 3,7 | 1,0 | 159 | | | | | |

*Notes: Event Number= Earthquake number assigned by IGN. Zs= Hypocentral depth. M= Ms magnitude. Lat = Latitude North. Lon=Longitude East. Smaj and Smin= Major and minor semi-axes of the location error elipse. Az= Azimuth of Smaj. * Depths are given only by CEA.*

Velocity structure of subsoil

Assuming a nearly vertical incidence of P and S body waves, we first estimated the mean shallow velocity structure. PGAL station is located at a depth of $Z_{PGAL}$=203.0 m below the surface level, in particular to PIAL station. Given this, we used the time arrivals of the P and S wavefronts at both stations, for each of the studied earthquakes, to obtain a mean estimate of the S wave travel time between both sites. Values from P arrivals were obtained assuming a Poisson ratio of ν=0.25. A summary of these observations is shown in Table 2.

Table 2. Estimated S wave velocities for each studied earthquake.

| Nº Event | Vp (km/s) | Vs* (km/s) | Vs‡ (km/s) |
|---|---|---|---|
| 885470 | 2,18 | 1,25 | 1,61 |
| 885487 | 2,636 | 1,52 | 1,57 |
| 885493 | 2,506 | 1,45 | 1,65 |
| 885494 | 2,743 | 1,58 | 1,269 |
| 890543 | 2,537 | 1,46 | 1,335 |
| 890840 | 2,942 | 1,7 | 1,585 |
| 891920 | 4,31 | 2,49 | 2,05 |
| 893160 | 3,076 | 1,76 | 1,664 |

*Notes: Vp= P wave velocity. Vs*= S wave velocity obtained from Vp (Vs=Vp/√3); Vs‡ S wave velocity from direct S wave arrival.*

From here, the mean S wave velocity for the shallowest 200 m can be set as *Vs*=1.5 km/s. We excluded event 891920 from the computation because it presents a relatively low signal to noise ratio. These velocities could be overestimated as they are not corrected for the vertical angle of incidence. From geothecnical studies (Rivas, *et al.,* 2011) and other seismic array studies using surface wave inversions, results suggest that at shallow depths less than 30m, S wave velocities could be lower than 1.0 km/s. Due to the observed uncertainties and the results from other studies, we assumed for this work a *Vs*=1.25 km/s.

RESULTS

For the computation of the displacement gradients using the seismo-geodetic method we selected PIAL as the reference station (station *"o"*). Given this, the results obtained with this method will be compared with those obtained using single-station estimates at the same station (PIAL). In Fig. 3 we show the resulting dynamic deformations for events 885487 and 890543. The P wave arrival is set in both cases 1.0 seconds after the beginning of the record. The S wave-group arrives about 0.7 after the P waves. Here it can be observed that the S waves produce the largest amplitudes of deformations.

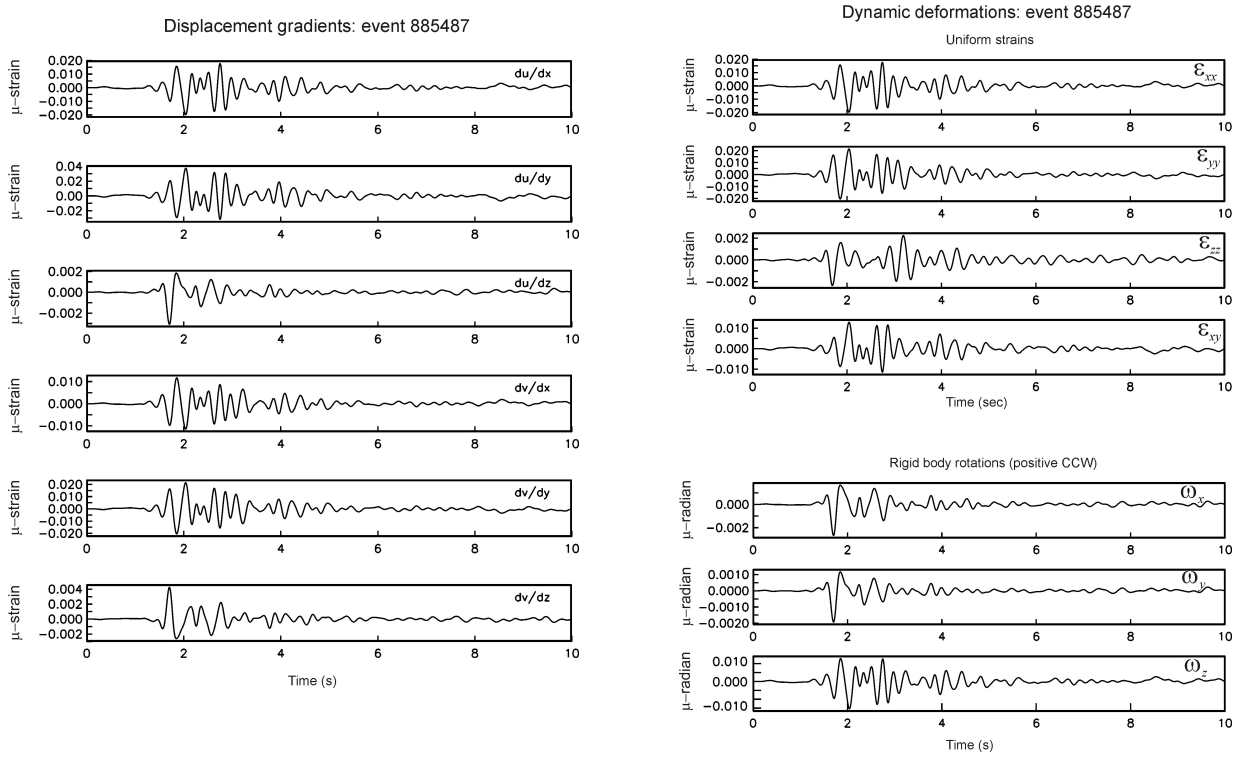


*Fig. 3. Displacement gradients and dynamic deformations (uniform strains and rigid body rotations) using the seismo-geodetic method for event 885487. Displacement gradients and uniform strains are in μ-strain and rotations in μ-radian. Positive rotations are in counterclockwise direction.*

For the case of the single-station estimates, we first obtained the set of angles ($\phi_k$, $\psi_k$) for the epicentral locations of each earthquake. To do this we assumed a homogeneous half space with the elastic properties previously obtained. We then computed the displacement gradients for each set of angles and earthquake. In all cases these gradients were computed using the data from the reference station PIAL. After comparing the results obtained using the initial locations for each earthquake, we observed that small changes in the epicentral location with respect to the station, produced large differences on the displacement gradients amplitudes, changing in some cases the polarity of the waveforms. This effect is mainly related with the angle of incidence of S waves. As this angle is nearly vertical, small changes of even few hundreds of meters in location can move the incident azimuth from one quadrant to another, changing the polarity of the displacement gradients. Magnitudes of the studied earthquakes are relatively low. Because of this, the epicentral locations were obtained using a relatively small number of stations. Additionally, only few temporal stations close to the studied region recorded these earthquakes. Given the absence of additional data to perform a more reliable relocation of earthquakes, we performed a constrained grid-search to improve their locations. This search was based on the analysis of polarities of the incident P waveforms and the relative amplitudes among the terms of the strain tensor components, obtained from the seismo-geodetic method.

The new epicenters were constrained to be located inside the intersection of the two error ellipses of the locations considered. If ellipses do not intersect, we look for the new location inside each ellipse separately (this is case of events 890543 and 885494). The differences between the new locations relative to the initial ones are always lower than 700 m. Once obtained these new locations for each event, we computed the strains and rotations using the new displacement gradients. Fig. 4 shows the comparison of the computed dynamic deformations (uniform strains and rigid body rotations) using the two studied methods for events 885487 and 890543. In this figure the results from the seismo-geodetic method are shown with solid lines and those obtained by the single-station method are shown with dashed lines. Differences were analyzed by

$$D = 100\frac{\sum_{k=1}^{N}\sqrt{[G_{i,j}^{s}(k\Delta t) - G_{i,j}^{g}(k\Delta t)]^2}}{A_{\max}\sqrt{N}} \tag{7}$$

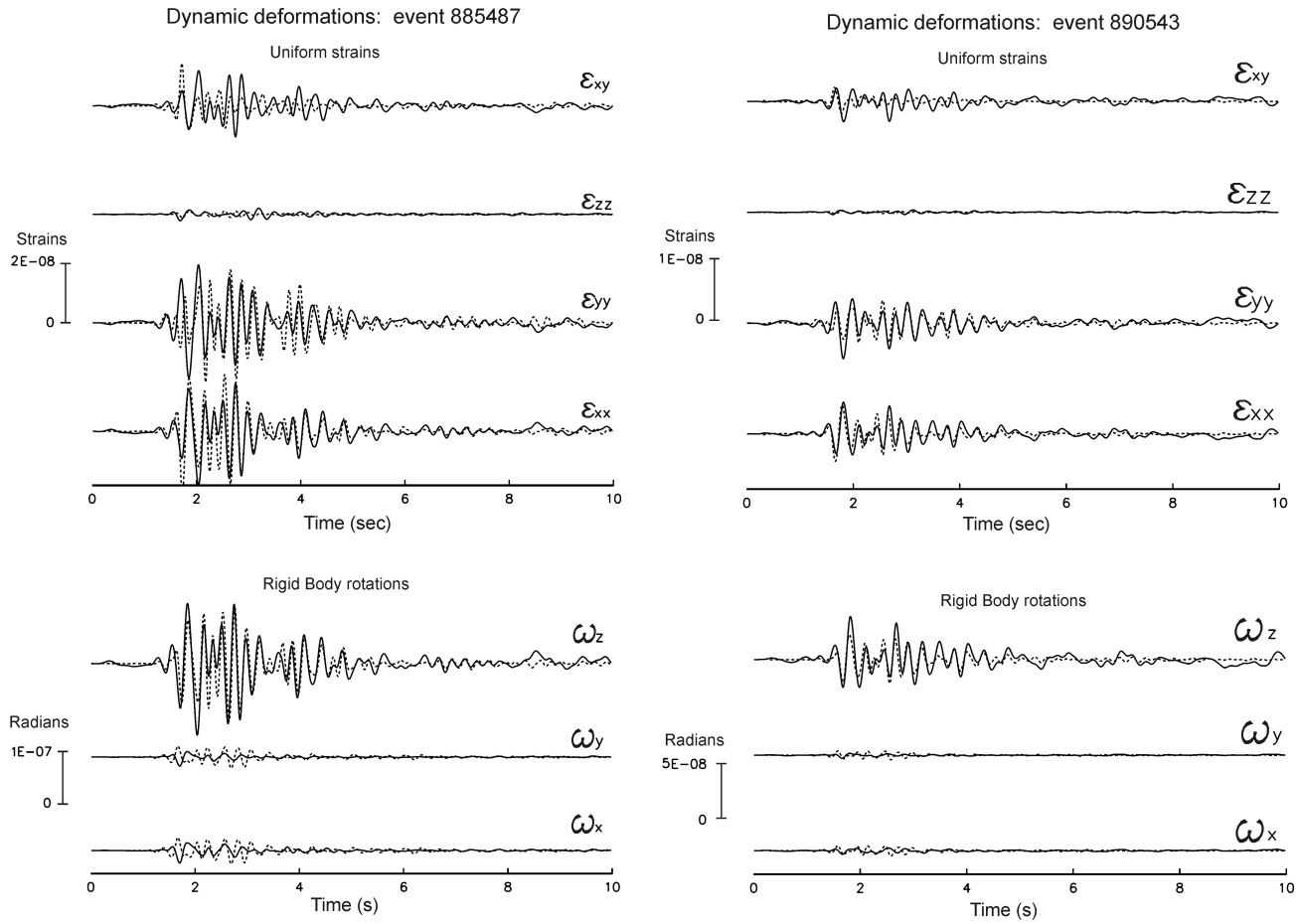


*Fig. 4. Comparison of the dynamic deformations (uniform strains and rigid body rotations) obtained by the two studied methods. Results from the seismo-geodetic method are shown with solid lines. Results obtained by single station estimates are shown with dashed lines. Comparisons for event 885487 are shown on the left hand side of the figure. For event 890543, comparisons are shown on the right hand side. Uniform strains are shown in strain units and rotations in radians. Positive rotations are in counterclockwise direction around axes.*

where $A_{max}$ is the absolute value of the maximum amplitude of each pair of compared time histories, $\Delta t$ is the time increment and $N$ is the total number of time samples. In this case, differences were measured for the S wave packet and excluding the coda of the time histories. Table 3 shows the values of D for each term of the strain tensor and for the eight events studied.

Table 3. Mean error -difference- (%) for each component of the strain tensor

| Comp | 885470 | 885487 | 885493 | 885494 | 890543 | 890840 | 891920 | 893160 |
|---|---|---|---|---|---|---|---|---|
| $\varepsilon_{xx}$ | 5.23 | 4.93 | 5.69 | 5.77 | 4.39 | 3.90 | 7.83 | 6.78 |
| $\varepsilon_{yy}$ | 7.87 | 6.02 | 7.58 | 8.82 | 3.97 | 5.21 | 13.07 | 6.93 |
| $\varepsilon_{zz}$ | 8.60 | 7.39 | 9.59 | 11.61 | 8.50 | 7.67 | 6.21 | 8.38 |
| $\varepsilon_{xy}$ | 7.22 | 7.08 | 7.55 | 7.11 | 6.68 | 6.03 | 10.21 | 9.80 |
| $\omega_x$ | 17.63 | 17.15 | 21.21 | 18.29 | 22.66 | 16.78 | 9.45 | 12.49 |
| $\omega_y$ | 17.51 | 19.20 | 20.87 | 21.75 | 20.76 | 17.85 | 8.12 | 14.98 |
| $\omega_z$ | 2.20 | 2.42 | 3.07 | 1.62 | 1.48 | 1.70 | 1.72 | 1.95 |

*Notes: Differences computed for all the strain tensor components for the 8 earthquakes studied. Comp= component of the strain tensor.*

## DISCUSSION AND CONCLUSIONS

Results show that the maximum amplitudes on the displacement gradients are mostly observed on $\partial u_1/\partial x_2$; in general, the horizontal components of the uniform strains, using both methods, systematically present larger amplitudes than the vertical ones. In the same way, rotations are larger around the vertical axis as they are given by the horizontal amplitudes of the displacement gradients. This result makes sense due to the type of incidence of the wave field. A way to interpret this is that because the earthquakes occurr very close to the stations, in particular to PIAL, the angle of incidence is small and the propagation direction is almost vertical. As the S waves deform the media in the transverse direction of propagation, the horizontal components should present larger amplitudes. As it can be seen from results, the best adjustment between both methods occurs during the arrival of the S waves. This could be because, for these values of incidence and distances, the S waves are less altered by scattering effects and geological irregularities.

On the other hand, from Table 3 it can be observed that the vertical components of strain and rotations present larger differences between traces from both methods, and that in general the horizontal components show lower differences. These values also show that the differences between methods are relatively low, suggesting that single-station estimates could be a good choice to estimate the dynamic deformations where only one three-component station is available.

## AKNOWLEDGMENTS

We wish to thank Confederación Hidrográfica del Ebro (CHE) for giving access to their facilities. This work was partially supported by Secretaría General para el Territorio y la Biodiversidad from Ministerio de Medio Ambiente, Rural y Marino, Spain, under grant 115/SGTB/2007/8.1, by EU with FEDER and by the research team RNM-194 of Junta de Andalucía, Spain. This work was done while M.A.S. was under the MICINN "Ramón y Cajal" subprogram contract (RYC-2010-05825; BOE-A-2010-2154), Spain.

## REFERENCES

Ariman, T. and M. Hamada [1981]. "Experimental investigations on seismic behavior of buried pipelines", in *Lifeline Earthquake Engineering,* D. J. Smith (Editor), Amer. Soc. Civil Eng., New York, 48-64.

Ayala, A. G. and M. J. O'Rourke [1989]. "Effects of the 1985 Michoacan Earthquake on water systems and other buried lifelines in Mexico". *National Center for Earthquake Engineering Research*; State University of New York at Buffalo. Technical Report NCEER-89-0009, -- 120 pp.

Bodin, P., J. Gomberg, S. K. Singh, and M. Santoyo [1997]. "Dynamic deformations of shallow sediments in the Valley of Mexico, Part I: Three-dimensional strains and rotations recorded on a seismic array", Bull. Seism. Soc. Am. 87, 528-539.

Clough, R. W. and J. Penzien [1993]. "*Dynamics of Structures",* B. J. Clark (Editor), Chap. 27, McGraw-Hill, New York, 704-710.

Gomberg J. [1997]. "Dynamic deformations and the M6.7, Northridge, California earthquake". Soil Dynam. and Earthq. Eng., Volume 16, Issues 7-8, 1997, Pages 471-494. doi:10.1016/S0267-7261(97)00011-0

Gomberg, J., and K. Felzer [2008]. "A model of earthquake triggering probabilities and application to dynamic deformations constrained by ground motion observations", J. Geophys. Res., 113, B10317, doi:10.1029/2007JB005184.

Gupta, H.K., [2002]. "A review of recent studies of triggered earthquakes by artificial water reservoirs with special emphasis on earthquakes in Koyna, India". Earth-Sci. Rev., 58 (3–4), 279–310.

Martinez-Garzón, P [2011]. "Deformaciones dinámicas originadas por sismos en presas: Caso de la presa de Itoiz (Navarra)". Master Thesis. Universidad Complutense de Madrid. Spain.

Martínez-Solares J.M., Mezcua J. [2003]. "*Catálogo sísmico de la península Ibérica (880 ac–1900)"*. Instituto Geográfico Nacional. Monografía N. 18 254pp.

Panel on Earthquake Engineering for Concrete Dams [1991]. "*Earthquake engineering for concrete dams: Design, performance and research needs"*. National Academy Press. Washington, D.C., USA. Pp. 158. ISBN 0-309-09336-0.

Rivas-Medina, A., Santoyo, M.A., Luzón, F., Benito, B., Gaspar-Escribano, J. M. and García-Jerez, A. [2011]. "Seismic Hazard and ground motion characterization at the Itoiz dam (Northern Spain)". Topical issue on Deformation and Gravity Change: Indicators of Isostasy, Tectonics, Volcanism and Climate Change Vol III, Pure Appl. Geoph. PAGEOPH. Accepted.

Ruiz, M., Gaspà, O., Gallart, J., Díaz, J., Pulgar, J.A., García-Sansegundo, J., López-Fernández,C., González-Cortina, J.M. [2006]. "Aftershocks series monitoring of the September 18, 2004 M=4.6 earthquake at the western Pyrenees: a case of reservoir-triggered seismicity?", Tectonophys., 424, 223–243. doi:10.1016/j.tecto.2006.03.037.

Singh, S. K., M. Santoyo, P. Bodin, and J. Gomberg [1997]. "Dynamic deformations of shallow sediments in the valley of Mexico, Part II: single station estimates", Bull. Seism. Soc. Am. 87, 540-550.

Spudich, P., L. K. Steck, M. Hellweg, J. B. Fletcher, and L. Baker [1995]. "Transient stresses at Parkfield, California, produced by the M 7.4 Landers earthquake of June 28, 1992: observations from the UPSAR dense seismograph array", J. Geophys. Res. 100, 675-690.

Talwani, P., [1997]. "On the nature of the reservoir-induced seismicity". Pure Appl. Geoph. PAHEOPH 150, 473–492.